Influence of accelerated corrosion on bi-material steel-CFRP double-lap joints bonded with thick adhesive

Pankaj.R. Jaiswal*, Rahul Iyer Kumar, Koen Rooms, Joren Rousseau, Kannaki Pondicherry, Wim De Waele

Soete Laboratory, Department of Electromechanical, Systems and Metal Engineering (EMSME), Ghent University, Belgium.

Abstract:

Bi-material steel-composite joints attract interest for marine applications. The marine environment imposes corrosion, which is a prolonged process. This work presents a two-electrode electrochemical setup for accelerating free corrosion of the steel surfaces of bi-material joints. It is used to study the impact of accelerated corrosion on the mechanical performance of bi-material double lap specimens subjected to quasi-static tensile testing. Several test series have been conducted to evaluate the influence of overlap length and bond line thickness on shear strength and failure mode.

Sixty specimens with a thick layer of methyl methacrylate (MMA) adhesive have been fabricated and cured at room temperature for at least 24 hours. Subsequently, thirty specimens were aged by subjecting them to electrochemical corrosion for 24 hours. All specimens were tested to failure in quasi-static tensile loading while monitoring the strain fields in the joint area using digital image correlation. The measurements reveal a homogeneous shear strain field at the onset of loading, with a rapidly increasing shear strain concentration near the edges of the bond line preceding final failure. Both a decrease in the adhesive thickness and an increase in the overlap length increase the

*Corresponding author: pankaj.jaiswal@ugent.be

shear strength. Higher shear strength was observed for the electrochemically aged specimens than that of non-aged specimens. This is attributed to the faster residual curing of the adhesive during ageing because an increasing percentage of copper ions (released from the anode) accelerates the curing of the MMA adhesive. The electrochemically aged specimens showed mixed failure modes, i.e. cohesive failure and adhesive failure at the interface between steel and adhesive, and skin failure within the composite laminates.

Keywords: Bi-material, adhesive joints, electrochemical corrosion, shear strength.

1. Introduction

Offshore and shipbuilding industries have been exploring technologies that reduce the weight of conventional, heavy loaded structures. Combining materials, such as steel and composites, can create a lighter and more robust structure. A 10% reduction in weight can increase the fuel efficiency by 8% (1), encouraging marine industries to use light-weight hybrid structures instead of considerably heavier single-metal structures. When joining materials with dissimilar properties, the use of adhesive bonding has clear advantages compared to riveting and bolting, namely low stress concentration (1–4), good static strength and damage tolerance (2), and good fatigue resistance (5–8). Optimum bonding technology can reduce the weight of structures by 15% (4). However, the long-term durability of adhesive joints in a saline environment remains a challenge and currently limits its use in marine applications. The durability of adhesive joints is highly dependent on environmental parameters such as moisture, temperature (4,9–11), salinity (12–16) and ultraviolet radiation (17–19).

The influence of moisture, temperature and salinity on the mechanical performance of double cantilever beam (DCB) specimens with a thin (<0.4mm) layer of epoxy adhesive, exposed for various durations up to 150 days, has been studied in (10,15,20,21). DCB specimens were fabricated by bonding aluminium alloy to aluminium alloy, CFRP to steel, and CFRP to CFRP. The results revealed that joint strength decreased significantly with increasing exposure time. This is acknowledged by Heshmati et al. (22–25), who conducted experimental and analytical studies to assess the effect of 1 year of exposure to different atmospheric conditions (salinity, moisture and temperature) on the durability of steel to FRP double lap joints bonded with a 1.5mm thick adhesive layer. Results showed substantial deterioration of the adhesive, causing a significant decrease in failure load of the joints. Arouche et al. (26) investigated the effect of salt spray ageing on the fracture toughness of composite to metal joints bonded with a thin (default) layer of epoxy adhesive and subjected to mixed-mode bending. Contrary to the observations reported higher, the aged specimens showed a 7 to 27 % rise in fracture toughness due to shear behaviour and plasticisation of the adhesive. Park et al. (27) studied the failure strength of CFRP single-lap joints bonded with a 0.092 mm thin epoxy adhesive layer subjected to three different environmental conditions, i.e. room temperature and dry (RTD), elevated temperature and wet (ETW), and cold temperature and dry (CTD) conditions. The ETW aged specimens showed considerable increase (11-23%), and the CTD aged specimens exhibited considerable decrease (8-21%) in the delamination strength of the laminate compared to RTD specimens. The influence of environmental exposure on the durability of steel-composite joints bonded with a thin epoxy layer is summarised in **Error! Reference source not found.**.

Table 1. Literature on steel / composite adhesive joints bonded with epoxy adhesive subjected to environmental exposure.

Ref.	Exposure parameters	Durations	Specimens	Adhesive	Adhesive thickness (mm)	Mechanical test
	Salt fog (5w% NaCl) spray chamber					
(14)	Wet and dry cycles: 6 hours salt spray followed by 18h in dry conditions, at 35°C.	0/2,500/5,000 and 10,000 hours	CFRP-steel double lap joints	Epoxy Sikadur-30	0.1	Tensile
(12)	Salt fog at 35°C.	2 weeks		Epoxy Araldite 420	0.5	Tensile, fatigue
(1)	Salt spray	30 and 90 days	Composite-steel double cantilever beam	Epoxy NVT201E®	0.4	Peel
(26)	Salt spray	137 days			Default	
	Salt water immersion					
(27)	Room temperature and dry, elevated temperature and wet (immersion immersed in water at 71^{o}C) and cold temperature at -54 ^{o}C and dry conditions	6 week	CFRP single-lap bonded joints	Epoxy adhesive FM300K	Default	Tensile
(28,29)	5 w% NaCl solution at 20, 40 and 50°C under static tensile load (20 % of ultimate load).	6 months	CFRP laminate and sheeting patched double-lap joints	Epoxy Araldite 420 /Araldite 2014	Default	Fatigue
	5 w% NaCl solution at 20 and 50°C under static tensile load (30% of yield stress of steel)	6 months	Single and double-sided tri-layered high modulus CFRP repaired steel plates	Epoxy Araldite 420	Default	Fatigue
(30)	Cycles of 10hrs wetting (3.5 w% NaCl) and 14hrs drying, followed by 300 fatigue cycles.	24 hours (0, 90 and 180 cycles)	CFRP-steel double lap joint	Epoxy	01	Fatigue

(31)	Cycles of 10hrs wetting (3.5 w% NaCl) and 14hrs drying			Epoxy Sikadur 30 and DZH		Tensile
(32)	1 week wet (5 w% NaCl at 38°C) and 1 week dry	up to 6 months		Epoxy	Default	Tensile
(33)	1) 5 w% NaCl at 20 and 50°C. 2) cyclic temperature 20 to 50°C and high level of relative humidity.	1 year		Epoxy Araldite 420	0.58	
	Low-temperature water bath					
(34)	Freeze-thaw cycles (−20°C to+20°C) and 50% RH.	10,000 hours	CFRP-steel double lap joint	Epoxy Sikadur 30	0.1	Tensile
(35)	3°C	3 and 6 months	CFRP strengthened tubular steel members	Epoxy Araldite K630	0.4	Four point bending
	Accelerated corrosion using electrochemical cell					
(36,37)	3.5 w% NaCl.	72 hours	CFRP-steel double lap joint	Epoxy BASF P4500.	Default	Tensile
(38)				Epoxy	Default	
(39)	2 w% NaCl at 40°C.	168 hours	steel-CFRP	Epoxy Proset	-	Mass loss
(40)		1000 and 3000 hours	Reinforced concrete beams and CFRP laminates	Epoxy Sikadur-Hex 103	Default	
(41)	5 w% NaCl at 50°C.	25 days	CFRP strengthened steel tubular member	Epoxy MBrace	0.4	Four-point bending

Most durability studies were carried out for environmental exposure of less than one year, whilst ship structures are designed for a service life of at least 25 years. An electrochemical process denoted as accelerated corrosion has been used to replicate the service life of steel-CFRP structures

in a corrosive environment (42). Batuwitage et al. (36,37) investigated the long term durability of CFRP-steel double lap bonded joints aged by electrochemical corrosion. The tensile strength of the aged CFRP-steel adhesive joints was significantly reduced, and CFRP rupture occurred. Likewise, Kim et al. (38) observed a noticeable reduction in tensile strength of aged CFRP-steel joints, driven by interfacial failure. Similar investigations have been conducted to evaluate the durability of hollow and solid CFRP-steel bonded beams (39–41). The results showed that accelerated corrosion adversely affects their strength and durability, especially when exposed to higher temperatures.

The above studies of CFRP-steel double lap joints mainly focused on the effects of environmental conditions (in particular accelerated corrosion) on their mechanical performance. However, the geometrical joint parameters such as overlap length, bond line thickness, adherend thicknesses could influence their strength. The durability of adhesive joints in a marine environment has mainly been studied using specimens with a (very) thin epoxy-based adhesive layer. These bond thicknesses are not representative of maritime applications, which is the focus of this study that was performed in the Qualify project of Interreg 2 Seas Mers Zeeën. One of the joint configurations studied in this project applies a very thick (multiple millimetres) two-component methyl methacrylate (MMA) adhesive layer for connecting a composite superstructure to the steel hull of the ship (2,43). The influence of accelerated corrosion on the mechanical performance of steel to CFRP joints bonded by a thick layer of ductile MMA adhesive has not yet been reported in the literature. Also, the effect of overlap length and adhesive thickness on their shear strength has not yet been studied. Therefore, this paper presents an experimental study to evaluate the mechanical behaviour of CFRP-steel double lap adhesive joints subjected to accelerated corrosion and subsequent quasi-static tensile testing. Two different boundary conditions, in terms of corrosion protection, have been implemented. The first allows free corrosion at the steel surface near the interface of steel and adhesive. The second additionally facilitates the diffusion of moisture in the

adhesive. Specimens were exposed to galvanic current when immersed in an electrolyte, which induced electrochemical corrosion reactions in an accelerated way. The deformations of the joint and strain distributions in the adhesive were evaluated using digital image correlation (DIC) (43,44) during tensile testing, followed by an evaluation of the failure modes.

2. Experiments

2.1 Materials and specimens

Following materials have been used to fabricate double lap joint (DLJ) specimens: S235 steel, CFRP, two-component MMA adhesive, and anti-corrosive primer and paint. The orthotropic CFRP sheet was composed of high strength, standard modulus 2x2 twill carbon fibre fabric and an epoxy matrix. It has a tensile strength of 600 MPa, Young's modulus of 70 GPa in longitudinal and transverse directions and an in-plane shear modulus of 5 GPa. The datasheet of the MMA adhesive reports a shear strength of 16-19 MPa and Young's modulus of 0.207-0.276 GPa. Sixty steel-CFRP double lap joints have been manufactured. All specimens consisted of two steel adherends (150 x 25 x 6 mm) (36), of which the surface has been sandblasted to an average roughness $R_a \cong 2.5$ μm, and treated with a cleaning agent (Loctite SF 7063) before bonding. CFRP straps of 25 mm wide were patched at each side using MMA adhesive. The specimens were cured at room temperature for at least 24 hours to attain the maximum shear strength. Figure 1 (a) illustrates the different DLJ specimen configurations, having an overlap length of 60, 80 and 100 mm and bond line thickness of 2, 4 and 6 mm. Three specimens were manufactured for each combination of overlap length and adhesive thickness.

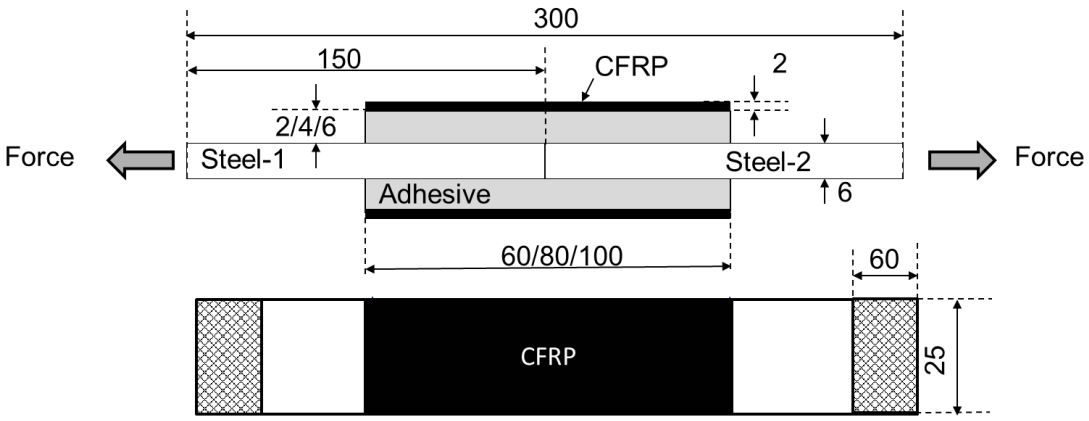

(a)

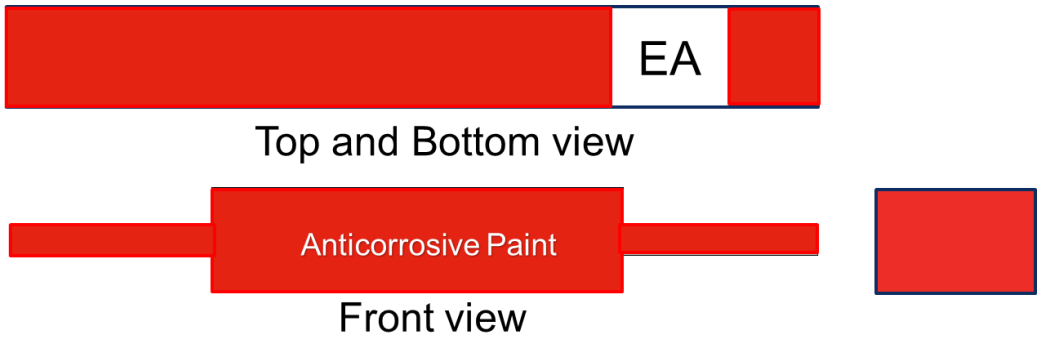

(b)

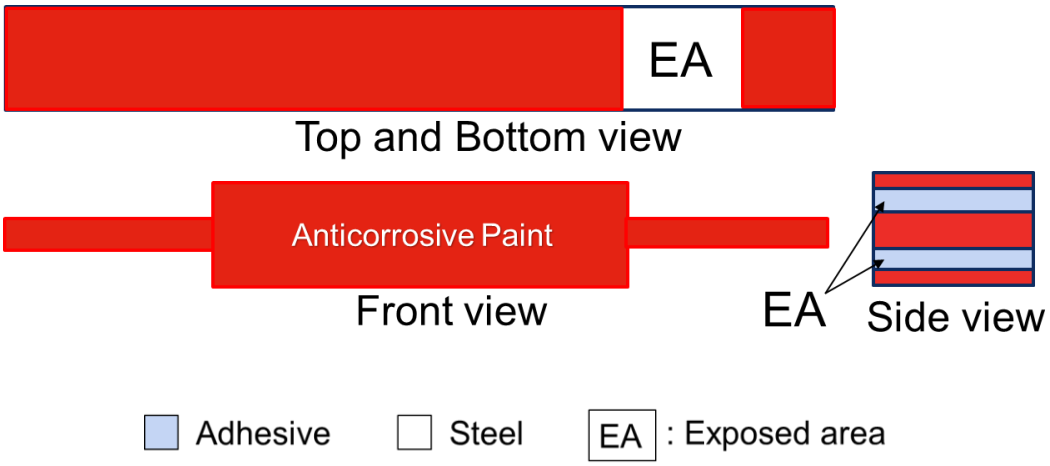

(c)

Figure 1 (a) Schematic representation of DLJ specimen (dimensions in mm) and (b) illustration of applied anti-corrosion paint boundary condition BC-1 and (c) BC-2.

Customised fixtures were designed to achieve edge-to-edge contact between the two steel adherends and to ensure perfect alignment of CFRP straps and adherends. The adhesive thickness and overlap length were controlled using different spacers. Recesses of 4 mm depth hold a surplus amount of adhesive to avoid shrinkage voids whilst curing under pressure (using a mass of 30 kg) for three hours. Following, specimens were removed from their fixture for residual curing for at least 24 hours at room temperature. Two different boundary conditions (BC-1 and BC-2) of applied anti-corrosion paint are detailed in Figure 1 (b,c). BC-1 was designed to study the effect of accelerated corrosion on the shear strength of DLJ specimens, only allowing uniform corrosion on the unprotected part of the steel. The design life of the ship, and thus of the studied joint, is 25 years. Every 5 years the ship is docked for inspection, maintenance and repair. The purpose of combining BC-1 with accelerated corrosion is to mimic the potential effect of damage to the anti-corrosive layer on the steel part of the joint that would remain unnoticed for a period in between two dockings. Since no corrosion travel was observed at the steel-adhesive interface for BC-1 (see section 4), a more severe boundary condition BC-2 was designed to additionally allow some diffusion of moisture through the adhesive. For that purpose, six specimens of the BC-1 configuration with the highest strength were fabricated. In the remainder of this paper, the aged specimens are identified as A-LxxTyy and the unaged as UA-LxxTyy with xx the overlap length in mm and yy the bond line thickness in mm.

2.2 Tensile testing

Three quasi-static tensile tests have been performed for each configuration of overlap length and bond line thickness on unaged and aged specimens, at a constant displacement rate of 1 mm/min and ambient temperature. Tests were performed on a servo-hydraulic testing machine MTS 810 with 50kN load cell and hydraulic wedge grips. Digital Image Correlation (DIC) instrumentation

was used to monitor joint deformation and strain in the adhesive by post-processing images in VIC-3D software. DIC instrumentation is based on a stereo camera system that captures images of the speckle pattern applied to the specimen's side surface. The procedures followed to create the speckle patterns and post-process the DIC images are explained in (2,43). Load, crosshead displacement and DIC data were recorded at 5Hz.

3. Accelerated ageing

3.1 Mass loss prediction

A Tafel experiment using a three-electrode setup (45) (see Figure 2) was performed to determine the corrosion current density (i_{corr}) of the steel adherend under free corrosion conditions in saltwater. The mean value of corrosion current density is determined as 12.60 μA/cm^2 (with a variation of 0.474); similar values have been reported for mild steel and martensitic steel (45,46). The corrosion current density (i_{corr}) value is used in Faraday's equation [1] to calculate the corrosion mass loss *r* in mils per year (47). Equations [2] and [3] (ASTM G102-89 (48)) are used to express mass loss in g/cm^2 or in mm.

$$r(in\ mpy) = 0.129\,\frac{\mathrm{a}i_{corr}}{\mathrm{nD}} \quad [1]$$

$$r\left(\frac{g}{cm2}\right) = r(in\ mpy)0.00254D \quad [2]$$

$$r\left(\frac{mm}{year}\right) = K_1\,\frac{i_{corr}}{D}\,EW \quad [3]$$

Where *a* is the atomic weight of the corroding metal (~56 grams for Fe), *n* is the number of electrons transferred in the oxidation reaction (2 for Fe^{2+}), *D* is the density of steel, *EW* is the equivalent weight of balance iron (gram), K_1 = 3.27 x 10 $^{-3}$ (mm g/μA cm yr), *m* is the mass of metal oxidised due to corrosion (gram).

In the context of the Qualify project, a corrosion loss representing 5 years of sea water exposure was aimed at, which corresponds to an interval in between two dockings at which the ship is inspected and repainted. Application of Faraday's law yields a theoretical mass loss of 8.48 g for the unprotected area of the steel substrate of the DLJ specimen during five years immersion in salt water at 24±1°C value.

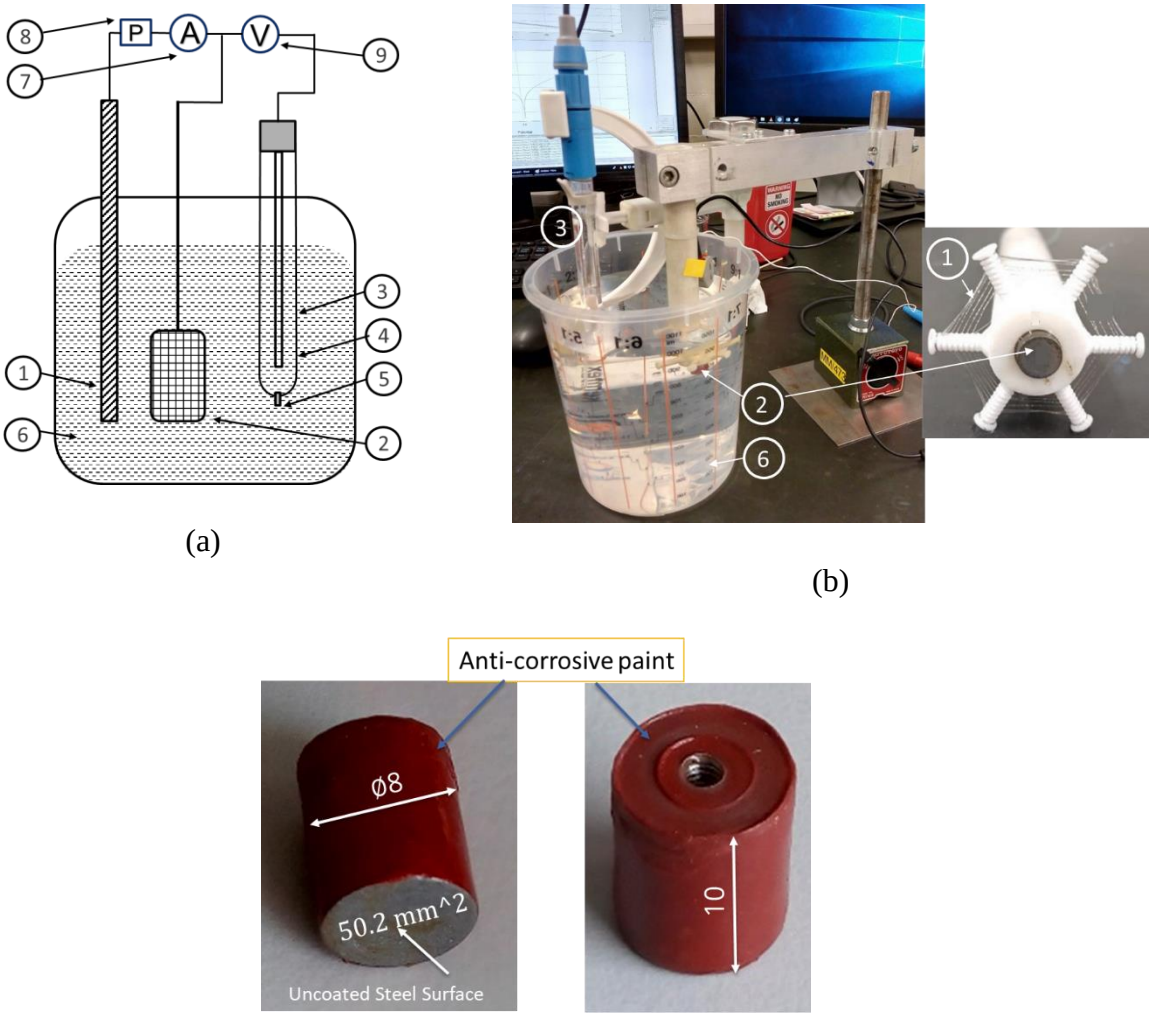

(a)

(b)

All dimensions are in mm

(c)

Figure 2 (a) Schematic of three electrode corrosion setup, (b) laboratory test setup and (c) working electrode (S235C). [1-counter electrode, 2-working electrode, 3-reference electrode, 4-AgCl, 5-porous junction, 6-electrolyte solution (artificial sea water), 7-ampère meter, 8-potentiostat, 9-volt meter].

3.2 Electrochemical corrosion

Corrosion of the DLJ specimens was accelerated using a two-electrode electrochemical corrosion setup, Figure 3. It consists of four essential components: anode, cathode, electrolyte and a DC power source. An S235 steel rod (diameter 25 mm and length 300 mm) was used as the cathode, and the DLJ specimen served as the anode, with free corrosion taking place at the unprotected steel substrate region leading to surface degradation due to loss of electrons. The two electrodes were connected to a DC potentiostat (capacity of 5 amperes) and placed in a plastic container filled with six litres of artificial seawater (ASTM D-1141-98) (49) acting as the electrolyte. The position of the anode is such that equal amounts of mass loss should occur at each specimen side.

Each specimen was individually placed in a plastic tank, and a separate DC potentiostat was used for each tank to avoid variations in electrical current during the accelerated corrosion process. After each experiment, the cathode was cleaned by a smooth wire brush and polishing paper, and the plastic container was thoroughly rinsed using a cleaning agent (Loctite SF 7063) and subsequently filled with fresh seawater. An electrical current intensity of 0.338 A was calculated based on equation [4] to achieve the higher calculated mass loss of 8.45 g in a time period of 24 hours.

$$m = \frac{\mathrm{Iat}}{\mathrm{nF}} \qquad [4]$$

I is the applied current (ampere), *F* is Faraday's constant (96,500 amperes/seconds), *t* is the reaction time (sec).

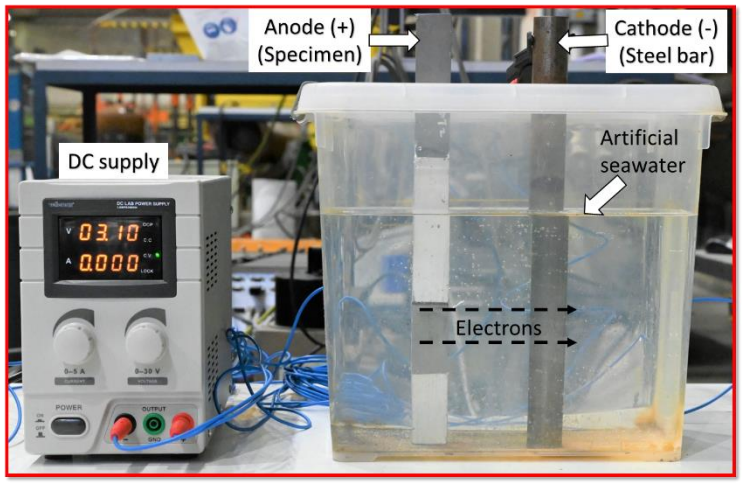

(a)

(b)

(c)

(d)

Figure 3 Electrochemical cells (a) and DLJ specimens: (b) unaged, (c) after 24 hours of ageing, (d) after an additional 6 hours of environmental exposure.

The condition of specimens before and after ageing are compared in Figure 3 (b) and (c), respectively. The immersed part of the specimen appeared dark black due to the formation of hydrated ferric oxide $Fe(OH)_2$ (38); after a few hours of environmental exposure, the colour turns brown due to oxidation. The corrosion process resulted in a local thickness reduction due to metal loss from the unprotected surface area. Following 24hrs exposure time, the sample was retrieved

and weighed without removing the corrosion products. Specimen mass was measured in a controlled environment using a weighing machine with an accuracy of 0.01 g. The experimental values (average of 3 identical specimens) of mass loss range from 7.71 to 8.14 g, which is slightly lower (3 to 8%) than the prediction.

4. Results and discussion

4.1 Tensile properties

As mentioned above, three unaged and three aged specimens were tested for each configuration of overlap length combined with adhesive thickness. The maximum, minimum and average tensile strengths are shown in Figure 4.

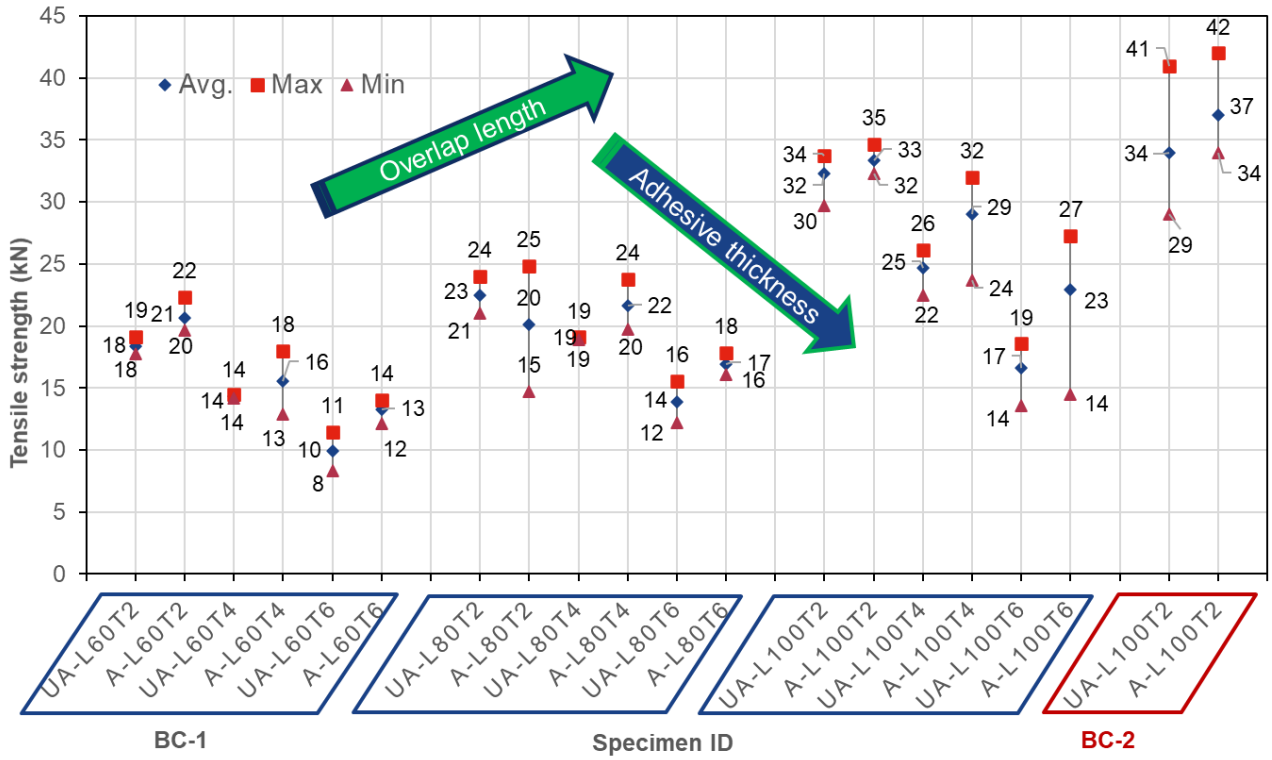

Figure 4. Tensile test results of aged and unaged specimens.

The results of tests performed on specimens with BC-1 are grouped in three categories with increasing overlap length (60, 80 and 100 mm), from left to right on the graph. Within each category, the thickness of the bond line increases from left to right (2, 4 and 6 mm). It can be observed that the tensile strength of the joints increases with increasing overlap length but decreases with increasing bond line thickness. First, increasing the bond thickness results in a higher probability of defects such as microvoids, air pockets and cracks in the adhesive bulk and thus decreases its cohesive strength. Second, numerical analysis of the stress state in tensile loaded joints has revealed larger stress concentration factors for thick joints (50), also contributing to lower failure strength. The electrochemically aged specimens showed, contrary to expectations, higher average tensile strengths (between 3 and 37 %) than the unaged specimens. The hypothesis put forward to explain this trend is that the anode releases different metal ions that react with the MMA adhesive and accelerate its residual curing during electrochemical corrosion. This is further discussed in Section 6. The load-elongation plots of aged specimens with 100 mm overlap length and 2 mm bond line thickness, having the highest shear strength, are shown in Figure 5 (a) up to the point of maximum load. A virtual DIC extensometer measures the displacement between two points on the steel substrates outside the adhesive region, Figure 5 (b). This displacement is the best estimate of the DLJ elongation.

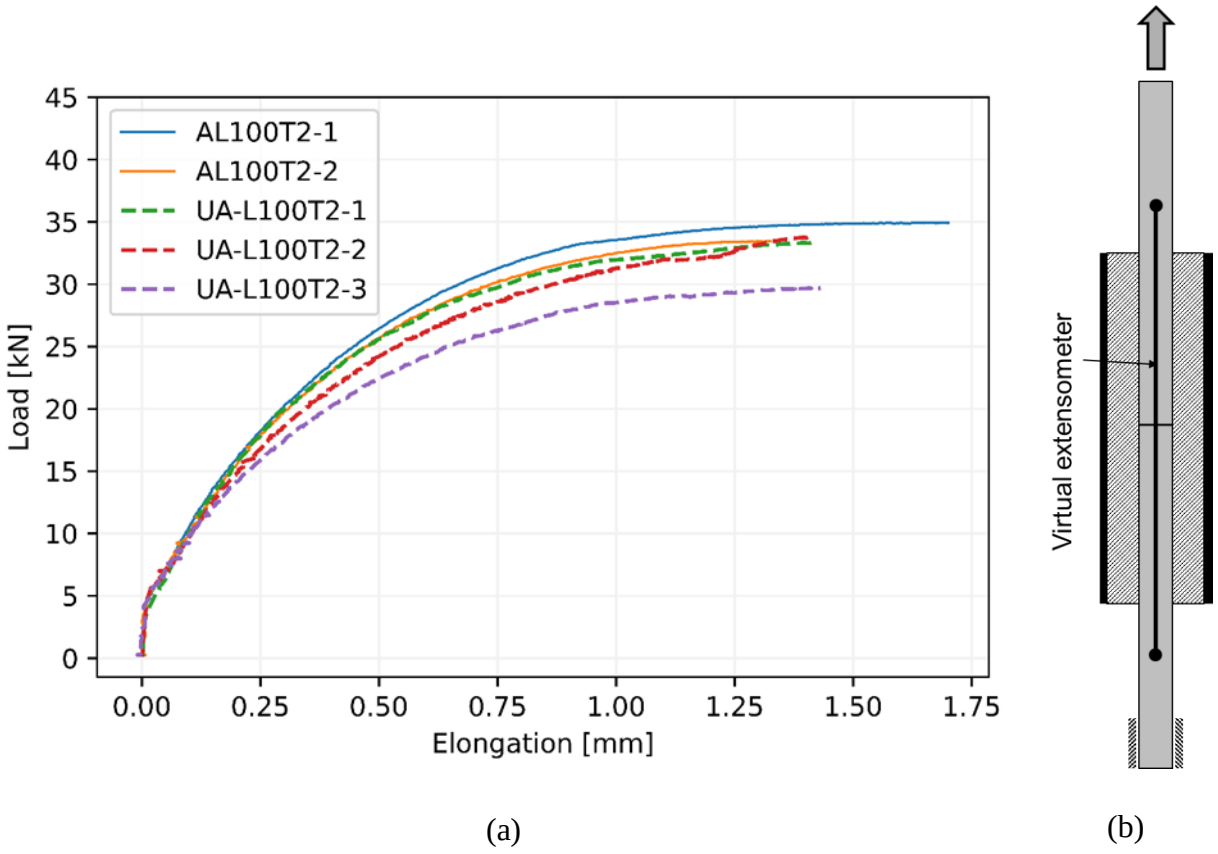

Figure 5 (a) Load/elongation plots of specimens UA-L100T2 and (b) virtual DIC extensometer to measure the joint extension.

The curves display a linear evolution until approximately 4 kN with minimal elongation of the joint. After that, the nonlinear behaviour of the curves is prominent, and the elongation significantly increases with constant load after approximately 1.1 mm extension. Similar average tensile strengths were recorded for aged and unaged specimens, 33 and 32 kN, respectively.

Almost all aged and unaged (BC-1) specimens showed a gradually increasing gap between the two steel adherends, followed by a sudden debonding of the steel-adhesive and adhesive-CFRP interfaces. The illustrated failure type is common in steel-CFRP double lap adhesive joints (33). The fracture surfaces of unaged and aged specimens of the joint configuration with the highest strength are demonstrated in Figure 6 (a,b).

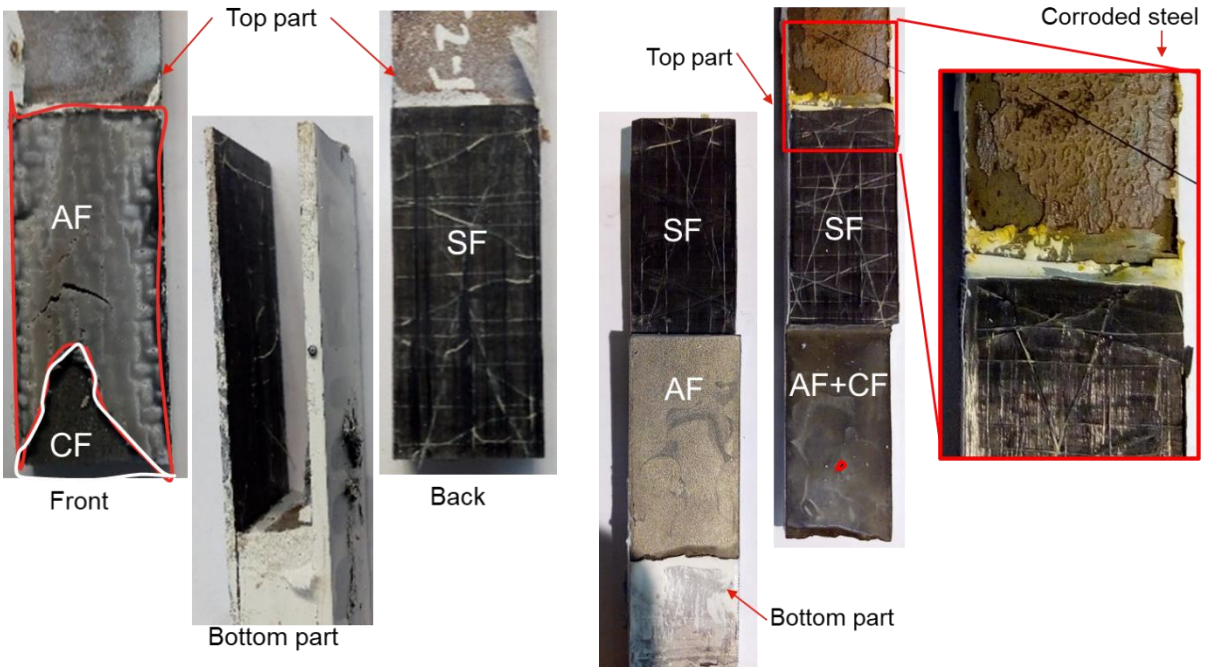

Figure 6 Failure mode of (a) unaged (UA-L100T2-1) and (b) aged (AL100T2-3) DLJ specimens of the highest strength configuration. AF: Adhesive failure, CF: Cohesive failure, SF: skin failure due to delamination of CFRP.

No interfacial corrosion was observed at the steel-adhesive interface in the aged specimen, whilst noticeable corrosion was observed on the steel part of the joint. No discolouration or damage to the CFRP sheets was observed, which shows that corrosion products originating from the steel were not deposited. Concerning the final rupture, the aged specimen showed adhesive and cohesive failure at the unaged (bottom) part of the specimen and skin failure due to CFRP delamination at the aged (upper) part of the specimen. The unaged specimen revealed mixed-mode (adhesive and cohesive) failure on the front and delamination of composite on the back face of the specimen. The failure modes suggest that the CFRP straps reached their maximum interlaminar strength capacity. Failure modes of the joints change with changes in bond line thickness. Almost all unaged and aged joints of 2 mm and 4 mm thick demonstrated adhesive and cohesive failure, whereas the 6 mm thick joints showed mostly adhesive failure. Evaluating strength and failure modes led to

conclude that there is no degradation of the adhesive or steel/adhesive interface due to electrochemical ageing.

4.2 Characterisation of strain evolution in the adhesive

First, specimen A-L100T2-5 is selected for a global analysis of the strain distribution of an aged specimen. The evolution of shear strain distribution is presented at different tensile load levels in Figure 7 (a).

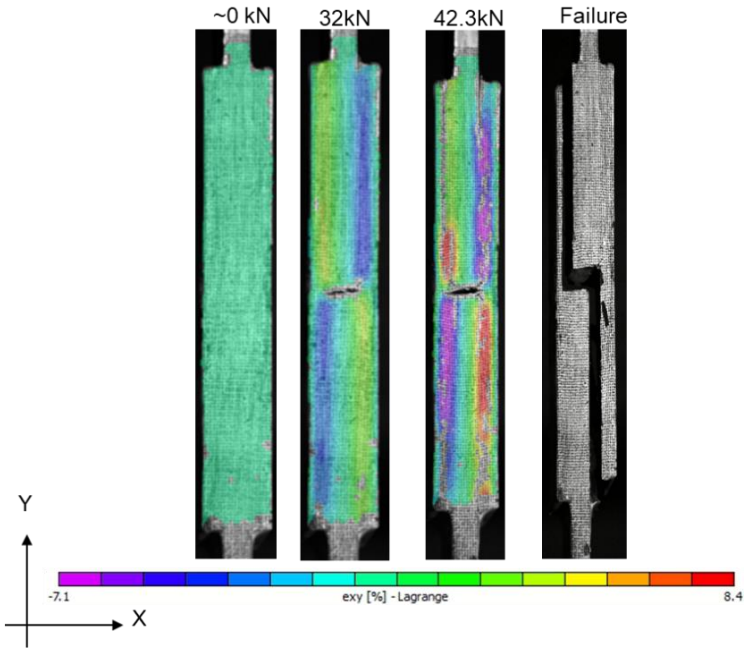

(a)

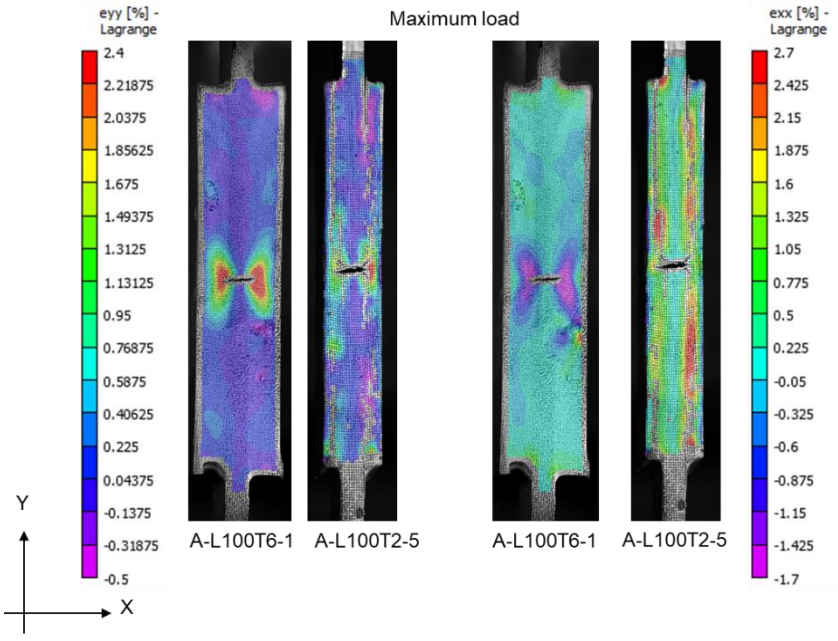

(b)

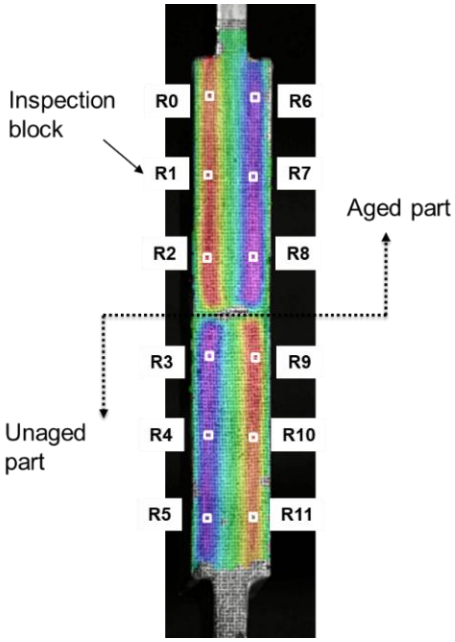

(c)

Figure 7 (a) Shear strain distribution and (b) longitudinal strain and peel strain distributions over the surface of an aged specimen (A-L100T2-5) and (c) Location of inspection blocks at the surface of the adhesive.

The first image in Figure 7 (a) is the reference image captured just before starting the test, and hence it refers to zero shear strain. The second image corresponds to a load level of 32 kN; the gap between two substrates increases and the bond lines show a significant strain development with maximum values occurring at the centre of the specimen. The third image corresponds to the maximum load during the test; significant damage initiated at the adhesive/composite and adhesive/steel interfaces at the upper left and right sides of the specimen. As a result, the shear strain pattern is non-homogeneous, contrary to the previous two images. Ultimately, the last image shows the specimen after the sudden failure of the interfaces. Similar types of shear strain distribution have been observed in all aged (BC-1 and BC-2) and unaged specimens.

Figure 7 (b) shows longitudinal and peel strain distributions at the cross-section of specimens with very thick (A-L100T6-1) and less thick (A-L100T2-5) adhesive bondlines at maximum load during the tensile tests. It can be concluded that a decreasing bond thickness results in more uniform strain distributions, hence this resulted in higher shear strength at failure.

Next, the values of local shear, normal and peel strains in the adhesive have been evaluated using an inspection block method during DIC post-processing, as shown in Figure 7(c). Twelve inspection blocks were placed along the bond lines of the joint (R0 to R5 on the right and R6 to R11 on the left side). Inspection blocks R0 to R2, R6 to R8 and R3 to R5, R9 to R11 were placed on the aged and unaged regions of the joint, respectively. The reported strain values of R0 to R11 are the average of the area within each inspection block. Figure 8 (a to f) shows, for each inspection block, the evolution of load versus local shear, normal and peel strain in the adhesive at both exposed and non-exposed sides of aged specimen A-L100T2-5 up to the point of failure.

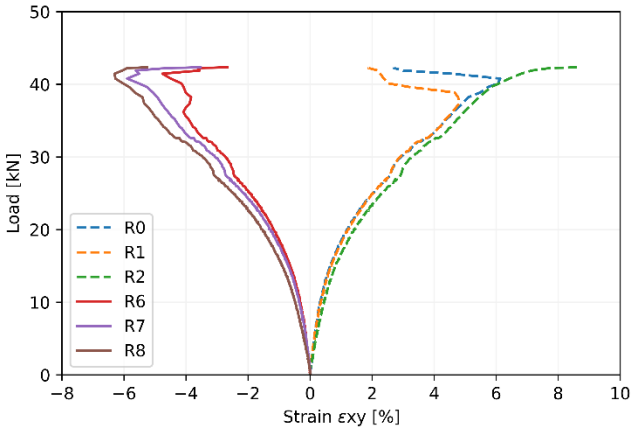

(a)

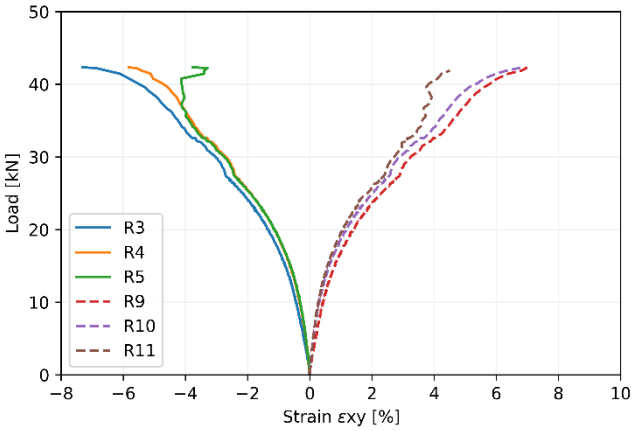

(b)

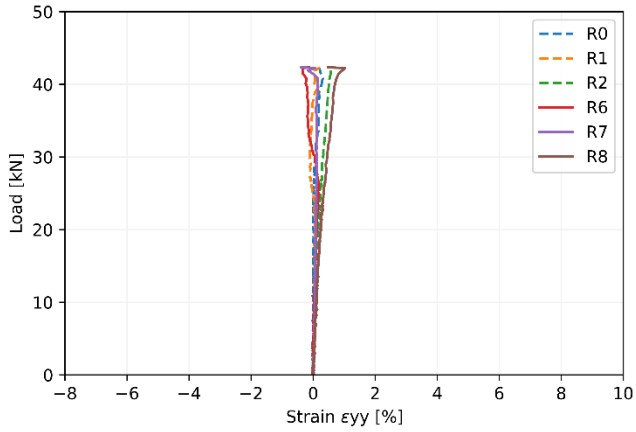

(c)

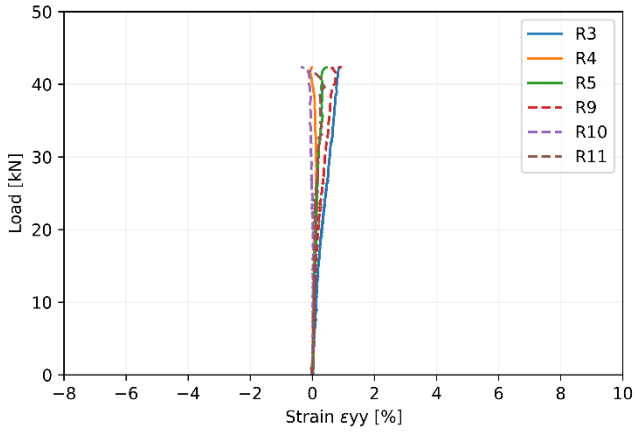

(d)

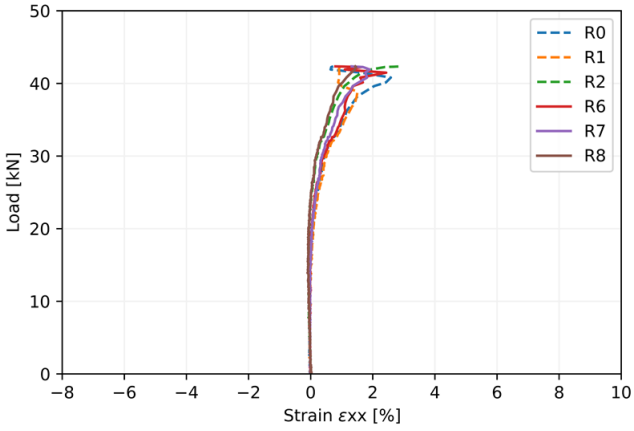

(e)

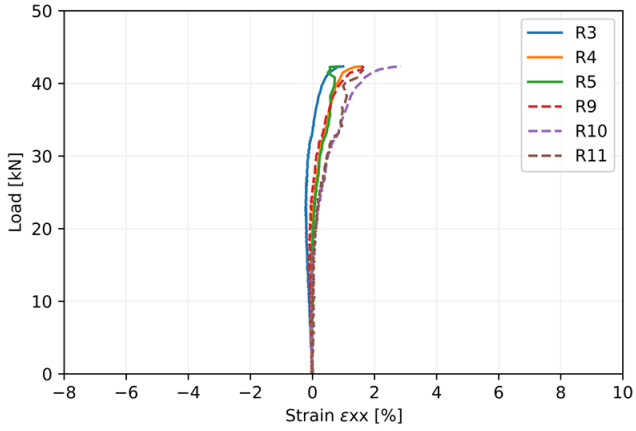

(f)

Figure 8 Curves of averaged shear stress versus (a,b) shear, (c,d) normal and (e,f) peel strain.

In Figure 8 (a, b), a general trend of increasing shear strain with increasing load can be seen until ~38 kN, and then shear strain values suddenly drop due to crack initiation at steel-adhesive and CFRP-adhesive interfaces at the upper right side of the joint. This trend is confirmed by observing the non-homogeneity of the shear strain pattern along the bond length at the interface of CFRP and adhesive on the top left side of the joint in the third image of Figure 7 (a). The shear strain values on the right side of the bond (locations R0 to R2 and R3 to R5) show a similar evolution. The shear strain evolutions at the left side of the joint at locations R6 to R8 and R9 to R11 are also similar but not identical. The shear strain at failure at locations R2, R8 and R3, R9 (middle part of the adhesive) is significantly higher than other locations.

The longitudinal strain (in the direction of the axial load) and the peel strain (perpendicular to the axial load) are evaluated for the same locations of interest in the adhesive, as shown in Figure 8 (c, d). These strain values are significantly lower than the shear strain values, showing the predominant shear loading of the adhesives. The local peel strain evolution for inspection blocks R0 to R5 is shown in Figure 8 (e, f). All curves display a linear evolution with negligible strain magnitude until 20 kN. A relatively significant increase in peel strain appears close to the onset of failure. By comparing local strain plots of aged and unaged parts of the joint, it can be concluded that the bond line at the aged and unaged part of the specimen experienced almost the same levels of local strain. In addition, the nominal shear strains in the adhesive have been evaluated using an inspection block method that covers the entire bond line beside one adherend of the specimen. The values of nominal shear stress are calculated by taking the ratio of tensile load to the sheared area (i.e., width multiplied by overlap length) of the joint. The mean, maximum and minimum values of nominal shear stress and strains at maximum load of aged (BC-1 and BC-2) and unaged specimens are tabulated in Table 2.

Table 2 Nominal shear stress and shear strain values at maximum load for aged and unaged DLJ specimens

Specimens	Global stress (MPa)			Shear strain (%)			Conditioned
	Mean	Maximum	Minimum	Mean	Maximum	Minimum	
Boundary condition BC-1							
UA-L60T2	11.9	12.0	11.6	8.4	10.5	6.5	
UA-L60T4	9.3	9.4	9.2	5.5	7.2	4.2	
UA-L60T6	5.7	6.2	5.3	3.3	4.2	1.7	
UA-L80T2	11.0	11.8	10.3	4.2	6.0	3.1	
UA-L80T4	9.3	9.4	9.2	5.3	6.1	4.4	Unaged
UA-L80T6	6.7	7.6	5.9	2.9	4.0	2.1	
UA-L100T2	12.7	13.3	11.7	9.3	11.3	8.1	
UA-L100T4	9.5	10.2	8.6	5.2	7.4	2.6	
UA-L100T6	9.5	10.2	8.6	2.5	3.1	1.6	
A-L60T2	11.6	12.5	10.4	6.1	6.8	5.6	
A-L60T4	10.3	11.8	8.6	4.8	6.8	2.0	
A-L60T6	8.8	9.3	8.1	3.0	3.1	2.8	
A-L80T2	11.5	12.4	10.4	4.0	5.0	2.6	
A-L80T4	10.9	11.9	10	6.0	6.4	5.5	Aged
A-L80T6	8.5	8.9	8.1	3.5	4.3	2.5	
A-L100T2	13.4	13.9	12.9	7.0	8.5	5.0	
A-L100T4	11.1	12.5	8.8	5.9	8.3	1.3	
A-L100T6	8.5	10.5	5.2	3.2	4.1	1.8	

Boundary condition BC-2							
UA-L100T2	8.5	10.1	7.2	7.5	8.5	6.6	Unaged
A-L100T2	9.3	10.5	8.5	4.0	5.0	4.0	Aged

Comparing the mean shear strain value at maximum load of unaged specimens (BC-1) led to conclude that the bond line of 2 mm thickness showed approximately 35 % and 55 % higher shear strain than 4 mm and 6mm thick adhesive joints, respectively. For the aged specimens, a 2 mm thick adhesive showed approximately 23 % and 39 % higher shear strain than 4 mm and 6mm thick adhesive, respectively. The best performing configuration (UA-L100T2) of unaged specimens showed 25 % and 47 % higher shear strain than the best performing aged specimens under the BC1 and BC-2, respectively.

5. Chemical analysis of electrolytic solution

As mentioned above, the electrochemically aged specimens showed higher shear strength than the unaged specimens. The hypothesis put forward to explain this trend is that during electrochemical ageing, the anode releases metal ions, which could react with the MMA adhesive and accelerate its residual curing. It is known that MMA based adhesives cure via a free radical mechanism (51). Transition metal salts based on Cu, Fe, Mn and others are sometimes added to the adhesive composition to increase reaction speed, i.e. they act as accelerators (52). For that reason, it has been hypothesised that the presence of such elements in the electrolytic solution can accelerate the residual curing of the MMA adhesive. A chemical analysis of both fresh and used electrolytic solutions (synthetic seawater) was performed using 25-millilitre solutions as per ISO 11885:2007 and CMA/2/I/B.1 standards. The inductively coupled plasma - optical emission spectrometry (ICP-

OES) technique was used after microwave destruction in nitric acid (HNO_3) to conduct element analysis. The analysis indicated less than 0.5, 0.1 and 1 mg/litre of Fe, Mn, and Cu, respectively, in fresh saltwater, while concentrations of 851, 4.07 and 0.310 mg/litre of Fe, Mn and Cu, respectively, were measured for the used electrolyte solution. Significantly higher concentrations found in the used electrolytic solution, support the hypothesis that the electrochemically aged specimens showed higher residual strength due to an accelerated residual cure of the MMA adhesive in the presence of Cu, Fe, and Mn. Recall that for BC-2 a large section of the adhesive of the double lap specimens is exposed to the electrolyte, whilst for BC-1 specimens this is limited to a scratch line, and the effects of residual curing are only expected for BC-2.

6. Conclusions

This paper discussed the effect of accelerated (electrochemical) corrosion on the strength of steel-CFRP double lap adhesive joints. The developed electrochemical corrosion procedure allows replicating five years of immersion of the steel adherend in salt water in a laboratory experiment of 24 hours. Predicted mass loss values based on Faraday's equation have been validated with experimental mass loss values.

The structural response and failure mode of specimens manufactured according to two different levels of corrosion protection have been evaluated and compared against unaged specimens. For a first series of joints, part of the steel adherend at one side of the specimen remained unprotected. The second series of joints also had part of the adhesive exposed to allow additional diffusion of electrolyte into the adhesive. Based on the experimental results, analyses and visual observations, the following conclusions are drawn.

1. The (residual) tensile strength of the joints increases with increasing overlap length and decreasing bond line thickness. Thinner bond lines lead to significantly higher values of critical shear strain, both in aged an unaged conditions.
2. The aged specimens have a residual tensile strength that is 3 to 37% higher than the unaged specimens. This observation was linked to the presence of copper ions in the electrolytic solution, which increases the residual curing of the MMA adhesive and thus leads to an increase in bond strength of the joint.
3. The observed failure modes of the joints changed with a change in bond line thickness. The specimens with 2 mm and 4 mm thick bond lines demonstrated adhesive and cohesive failure at the interface of steel and adhesive and delamination of the composite near the adhesive-CFRP interface. However, 6 mm thick bond line specimens showed adhesive failure at the steel-adhesive or composite-adhesive interface due to non uniform peel and longitudinal strain distributions in the adhesive.

Acknowledgement and funding

The authors would like to acknowledge Dr. Tatiana Stefanov (M2i, the Netherlands) for her valuable contribution to understanding the chemical background of adhesives.

This research is part of the project “QUALIFY–Enabling Qualification of Hybrid Joints for Lightweight and Safe Maritime Transport” and received funding from the Interreg2Seas programme 2014-2020 co-funded by the European Regional Development Fund under subsidy contract No 03-051 and the province of East-Flanders.

References

1. Teixeira de Freitas S, Banea MD, Budhe S, de Barros S. Interface adhesion assessment of composite-to-metal bonded joints under salt spray conditions using peel tests. Compos Struct. 2017;164:68–75.
2. Jaiswal PR, Kumar RI, Saeedifar M, Saleh MN, Luyckx G, De Waele W. Deformation and damage evolution of a full-scale adhesive joint between a steel bracket and a sandwich panel for naval application. Proc Inst Mech Eng Part C J Mech Eng Sci. 2020;
3. Saeedifar M, Saleh MN, De Freitas ST, Zarouchas D. Damage characterization of adhesively-bonded Bi-material joints using acoustic emission. Compos Part B Eng. 2019;176(August):107356.
4. Hirulkar NS, Jaiswal PR, Reis PNB, Ferreira JAM. Bending strength of single-lap adhesive joints under hygrothermal aging combined with cyclic thermal shocks. J Adhes. 2019;00(00):1–15.
5. Zuo P, Vassilopoulos AP. Review of fatigue of bulk structural adhesives and thick adhesive joints. Int Mater Rev. 2021;66(5):313–38.
6. Chataigner S, Wahbeh M, Garcia-Sanchez D, Benzarti K, Birtel V, Fischer M, et al. Fatigue Strengthening of Steel Bridges with Adhesively Bonded CFRP Laminates: Case Study. J Compos Constr. 2020;24(3):05020002.
7. Mariam M, Afendi M, Abdul Majid MS, Ridzuan MJM, Azmi AI, Sultan MTH. Influence of hydrothermal ageing on the mechanical properties of an adhesively bonded joint with different adherends. Compos Part B Eng. 2019;165(November 2018):572–85.
8. Mu W, Qin G, Na J, Tan W, Liu H, Luan J. Effect of alternating load on the residual strength of environmentally aged adhesively bonded CFRP-aluminum alloy joints.

Compos Part B Eng. 2019;168(August 2018):87–97.

9. Hirulkar NS, Jaiswal PR, Reis PNB, Ferreira JAM. Effect of hygrothermal aging and cyclic thermal shocks on the mechanical performance of single-lap adhesive joints. Int J Adhes Adhes. 2020;99:102584.
10. Viana G, Costa M, Banea MD, da Silva LFM. Moisture and temperature degradation of double cantilever beam adhesive joints. J Adhes Sci Technol. 2017;31(16):1824–38.
11. Andrade B, Souza JPB, Reis JML, da Costa Mattos HS. A temperature-dependent global failure criterion for a composite/metal joint. Compos Part B Eng. 2018;137(November 2017):278–86.
12. Yu QQ, Gao RX, Gu XL, Zhao XL, Chen T. Bond behavior of CFRP-steel double-lap joints exposed to marine atmosphere and fatigue loading. Eng Struct. 2018;175(1239):76–85.
13. Papanicolaou GC, Charitidis P, Mouzakis DE, Karachalios E, Jiga G, Portan D V. Experimental and numerical investigation of balanced Boron/Epoxy single lap joints subjected to salt spray aging. Int J Adhes Adhes. 2016;68:9–18.
14. Yang Y, Silva MA, Silva RJC. Material degradation of cfrp-to-steel joints subjected to salt fog. Compos Part B Eng. 2019;173(January):106884.
15. Arouche MM, Budhe S, Alves LA, Teixeira de Freitas S, Banea MD, de Barros S. Effect of moisture on the adhesion of CFRP-to-steel bonded joints using peel tests. J Brazilian Soc Mech Sci Eng. 2018;40(1):1–8.
16. Li H, Zhang K, Cheng H, Suo H, Cheng Y, Hu J. Multi-stage mechanical behavior and failure mechanism analysis of CFRP/Al single-lap bolted joints with different seawater ageing conditions. Compos Struct. 2019;208(October 2018):634–45.
17. Amorim FC, Reis JML, Souza JFB, da Costa Mattos HS. Investigation of UV exposure in

adhesively bonded single lap joints. In: Applied Adhesion Science. Springer International Publishing; 2018.

18. Jaiswal PR, Hirulkar NS, Reis PNB, Papadakis L, Khan SN. Effect of cyclic solar (UV) radiation and temperature on mechanical performance of single lap adhesive joint. In: 2017 International Conference on Intelligent Computing, Instrumentation and Control Technologies, ICICICT 2017. 2018. p. 182–9.
19. Nguyen TC, Bai Y, Zhao XL, Al-Mahaidi R. Effects of ultraviolet radiation and associated elevated temperature on mechanical performance of steel/CFRP double strap joints. Compos Struct. 2012;94(12):3563–73.
20. Arouche MM, Budhe S, Banea MD, Teixeira de Freitas S, de Barros S. Interlaminar adhesion assessment of carbon-epoxy laminates under salt water ageing using peel tests. Proc Inst Mech Eng Part L J Mater Des Appl. 2019;233(8):1555–63.
21. Fernandes P, Viana G, Carbas RJC, Costa M, da Silva LFM, Banea MD. The influence of water on the fracture envelope of an adhesive joint. Theor Appl Fract Mech. 2017;89:1–15.
22. Heshmati M, Haghani R, Al-Emrani M, André A. On the strength prediction of adhesively bonded FRP-steel joints using cohesive zone modelling. Theor Appl Fract Mech. 2018;93:64–78.
23. Heshmati M, Haghani R, Al-Emrani M. Durability of CFRP/steel joints under cyclic wet-dry and freeze-thaw conditions. Compos Part B Eng. 2017;126:211–26.
24. Heshmati M, Haghani R, Al-Emrani M. Effects of moisture on the long-term performance of adhesively bonded FRP/steel joints used in bridges. Compos Part B Eng. 2016;92:447–62.
25. Heshmati M, Haghani R, Al-Emrani M. Environmental durability of adhesively bonded

FRP/steel joints in civil engineering applications: state of the art. Compos Part B Eng. 2015;81:259–75.

26. Arouche MM, Saleh MN, Teixeira de Freitas S, de Barros S. Effect of salt spray ageing on the fracture of composite-to-metal bonded joints. Int J Adhes Adhes [Internet]. 2021;108(April):102885. Available from: https://doi.org/10.1016/j.ijadhadh.2021.102885

27. Park Y Bin, Song MG, Kim JJ, Kweon JH, Choi JH. Strength of carbon/epoxy composite single-lap bonded joints in various environmental conditions. Compos Struct [Internet]. 2010;92(9):2173–80. Available from: http://dx.doi.org/10.1016/j.compstruct.2009.09.009

28. Borrie D, Zhao XL, Singh Raman RK, Bai Y. Fatigue performance of CFRP patched pre-cracked steel plates after extreme environmental exposure. Compos Struct. 2016;153:50–9.

29. Borrie D, Liu HB, Zhao XL, Singh Raman RK, Bai Y. Bond durability of fatigued CFRP-steel double-lap joints pre-exposed to marine environment. Compos Struct. 2015;131:799–809.

30. Wang Y, Li J, Deng J, Li S. Bond behaviour of CFRP/steel strap joints exposed to overloading fatigue and wetting/drying cycles. Eng Struct. 2018;172(June):1–12.

31. Wang Y, Zheng Y, Li J, Zhang L, Deng J. Experimental study on tensile behaviour of steel plates with centre hole strengthened by CFRP plates under marine environment. Int J Adhes Adhes. 2018;84(February):18–26.

32. Dawood M, Rizkalla S. Environmental durability of a CFRP system for strengthening steel structures. Constr Build Mater. 2010;24(9):1682–9.

33. Nguyen TC, Bai Y, Zhao XL, Al-Mahaidi R. Durability of steel/CFRP double strap joints exposed to sea water, cyclic temperature and humidity. Compos Struct. 2012;94(5):1834–45.

34. Yang Y, Silva MAG, Biscaia H, Chastre C. Bond durability of CFRP laminates-to-steel

joints subjected to freeze-thaw. Compos Struct. 2019;212(January):243–58.

35. Kabir MH, Fawzia S, Chan THT, Gamage JCPH. Comparative durability study of CFRP strengthened tubular steel members under cold weather. Mater Struct Constr. 2016;49(5):1761–74.

36. Batuwitage C, Fawzia S, Thambiratnam D, Al-Mahaidi R. Durability of CFRP strengthened steel plate double-strap joints in accelerated corrosion environments. Compos Struct. 2017;160:1287–98.

37. Batuwitage C, Fawzia S, Thambiratnam D, Al-Mahaidi R. Evaluation of bond properties of degraded CFRP-strengthened double strap joints. Compos Struct. 2017;173:144–55.

38. Kim YJ, Bumadian I, Park J-S. Galvanic Current Influencing Interface Deterioration of CFRP Bonded to a Steel Substrate. J Mater Civ Eng. 2016;28(2):04015129.

39. Arronche L, Gordon K, Ryu D, La Saponara V, Cheng L. Investigation of galvanic corrosion between AISI 1018 carbon steel and CFRPs modified with multi-walled carbon nanotubes. J Mater Sci. 2013;48(3):1315–23.

40. Badawi M, Soudki K. Control of Corrosion-Induced Damage in Reinforced Concrete Beams Using Carbon Fiber-Reinforced Polymer Laminates. J Compos Constr. 2005;9(2):195–201.

41. Kabir MH, Fawzia S, Chan THT, Badawi M. Durability of CFRP strengthened steel circular hollow section member exposed to sea water. Constr Build Mater. 2016;118:216–25.

42. Tavakkolizadeh BM, Member S, Saadatmanesh H. Galvanic corrosion of carbon and steel in aggressive environments. 2001;(August):200–10.

43. Jaiswal PR, Kumar RI, De Waele W. Unified methodology for characterisation of global fatigue damage evolution in adhesively bonded joints. Frat ed Integrita Strutt.

2020;14(53):26–37.

44. Dispersyn J, Hertelé S, Waele W De, Belis J. Assessment of hyperelastic material models for the application of adhesive point-fixings between glass and metal. Int J Adhes Adhes. 2017;77(March):102–17.

45. Pondicherry K, Vancoillie J, De Pauw J, Sukumaran J, Fauconnier D, De Baets P. Design and development of a novel electrochemical abrasion-corrosion tester. Tribol Int. 2019;131:652–60.

46. Wang XY, Li DY. Application of an electrochemical scratch technique to evaluate contributions of mechanical and electrochemical attacks to corrosive wear of materials. Wear. 2005;259(7–12):1490–6.

47. Jones DA. Principles and prevention of corrosion. Second Edi. Prentice Hall, Upper Saddle River, NJ 07458; 1996.

48. Astm G 102. Standard Practice for Calculation of Corrosion Rates and Related Information. Vol. 89, Astm G 102. 1999. p. 1–7.

49. ASTM D1141. Standard Practice for the Preparation of Substitute Ocean Water. ASTM Int. 2013;98(Reapproved 2013):1–3.

50. Daviesa.P, L. Sohierb, J.-Y. Cognardc, A. Bourmaudd, D. Choqueusea ER and RC. Influence of adhesive bond line thickness on joint strength of composite aircraft structures. J Phys Conf Ser. 2021;1925(1):724–36.

51. Dillard DA. Advances in structural adhesive bonding. Woodhead Publishing Limited; 2010.

52. Strand RM. Patent Application Publication. Vol. 1. US; US 2010/0113674 A1, 2010.